Comput Geosci (2016) 20:525–540
DOI 10.1007/s10596-015-9503-x

ORIGINAL PAPER

Ensemble level upscaling for compositional flow simulation

Hangyu Li[1] **· Louis J. Durlofsky**[1]

Received: 21 October 2014 / Accepted: 11 May 2015 / Published online: 13 June 2015

Abstract Uncertainty quantification is typically accomplished by simulating multiple geological realizations, which can be very expensive computationally if the flow process is complicated and the models are highly resolved. Upscaling procedures can be applied to reduce computational demands, though it is essential that the resulting coarse-model predictions correspond to reference fine-scale solutions. In this work, we develop an ensemble level upscaling (EnLU) procedure for compositional systems, which enables the efficient generation of multiple coarse models for use in uncertainty quantification. We apply a newly developed global compositional upscaling method to provide coarse-scale parameters and functions for selected realizations. This global upscaling entails transmissibility and relative permeability upscaling, along with the computation of α-factors to capture component fluxes. Additional features include near-well upscaling for all coarse parameters and functions, and iteration on the α-factors, which is shown to improve accuracy. In the EnLU framework, this global upscaling is applied for only a few selected realizations. For 90 % or more of the realizations, upscaled functions are assigned statistically based on quickly computed flow and permeability attributes. A sequential Gaussian co-simulation procedure is incorporated to provide coarse models that honor the spatial correlation structure of the upscaled properties. The resulting EnLU procedure is applied for multiple realizations of two-dimensional models, for both Gaussian and channelized permeability fields. Results demonstrate that EnLU provides P10, P50, and P90 results for phase and component production rates that are in close agreement with reference fine-scale results. Less accuracy is observed in realization-by-realization comparisons, though the models are still much more accurate than those generated using standard coarsening procedures.

Keywords Upscaling · Scale up · Multiscale · Reservoir simulation · Uncertainty quantification · Compositional flow · EOR · Near-well upscaling

1 Introduction

Uncertainty quantification is an essential component of reservoir management. To assess the effects of uncertainty, multiple highly-resolved geological realizations are generated, and flow simulation is performed for each model. This results in high computational costs, especially for compositional systems, which involve complex physics and many unknowns. Upscaling can be applied to reduce the computational demands, though the coarsening procedure must ensure that the resulting flow models provide predictions of sufficient accuracy relative to fine-scale models. When the goal is uncertainty quantification, realization-by-realization agreement may be less important than accuracy in key flow statistics, such as the P10, P50, and P90 responses for oil, gas, or component production rates (here the P10 rate indicates the rate corresponding to the tenth percentile of the cumulative distribution function, and similarly for P50 and P90 rates).

✉ Hangyu Li
hangyu.li@shell.com

[1] Department of Energy Resources Engineering, Stanford University, Stanford, CA 94305, USA

In this paper, we develop an ensemble level upscaling (EnLU) procedure for uncertainty quantification for compositional systems. The objective is to efficiently compute flow statistics using a limited amount of fine-scale simulation combined with a large number of inexpensive coarse-scale simulations. To achieve the required level of accuracy, we apply a newly developed global upscaling approach, which includes transmissibility and relative permeability upscaling for flow and transport effects, and computation of α-factors (discussed below) to capture component fluxes. Specialized near-well upscaling, for the computation of coarse-scale well index, relative permeability, and α-factors for well models, is also performed. This detailed compositional upscaling is applied only to a few selected realizations. For the bulk (90 % or more) of the realizations, upscaled relative permeabilities and α-factors are assigned statistically. This assignment is based on quickly-computed 'attributes,' which are determined for each coarse interface in each realization during single-phase upscaling. A geostatistical sequential Gaussian co-simulation procedure is used in conjunction with the attributes to assign coarse-scale properties for new realizations, in a manner that honors the spatial correlation structure of the upscaled properties.

We now briefly discuss existing upscaling procedures for single-phase, two-phase, and compositional flow parameters, with emphasis on the methods that are most relevant to this work. A wide variety of upscaling methods have been developed to compute coarse-scale permeability or transmissibility. In this work, we apply a global transmissibility upscaling method, which requires the solution of the global single-phase pressure equation, since this approach generally provides the highest level of accuracy. Global transmissibility upscaling procedures have been presented in, e.g., [1–4]. The latter two papers [3, 4] applied iteration to improve the accuracy of the upscaled transmissibilities, and a related approach will be implemented here in our compositional upscaling. Most global upscaling procedures are applicable for two-point flux approximations, though the methods developed in [4] are applicable for multipoint flux approximations.

Multiphase upscaling involves the computation of coarse-scale relative permeability curves. Global methods are computationally demanding since they require the time-dependent solution of the full problem, though they can still be useful when the upscaled functions can be reused in subsequent simulations. Recent global and local-global methods, applicable for use with the transmissibility upscaling procedures noted above, have been presented in [5–7]. A variety of earlier two-phase upscaling procedures are discussed in [8–11].

The near-well region typically requires specialized treatment in upscaling procedures. Such techniques were first developed within the context of transmissibility upscaling in [12]. Later extensions were presented in [2, 13, 14], among others. Recent two- and three-phase near-well upscaling procedures have been presented in [15–18]. These papers demonstrated the important mobility effects that must be captured in near-well upscaling to assure accuracy in coarse-scale well rates.

Upscaling procedures for compositional simulations have also been developed. In [19], the 'pseudo K-value' method was introduced to capture differences in composition between fine- and coarse-scale models. Fayers et al. [20] developed a dual zone mixing model, which requires two flash calculations for each coarse grid block. In subsequent work, Barker and Fayers [21] simplified this model and introduced so-called α-factors to correct component fluxes through coarse-scale interfaces. In [22], streamline techniques were applied to provide fine-scale information for use in computing the α-factors. This approach was used for field cases in [23], though this work only considered relatively simple sector models in which the flow was largely single-phase. The computation of α-factors for three-dimensional fractured reservoirs with gravity and capillarity was accomplished in [24], though again the flow was essentially single-phase. Global compositional upscaling methods based on nonequilibrium thermodynamics have also been developed [25, 26], and thermodynamically consistent α-factors were derived using this approach [25]. It is important to note, however, that none of the compositional upscaling procedures discussed here has included treatments for the near-well region. Based on earlier findings for two- and three-phase flow problems, we expect this to be an essential component of any practical compositional upscaling methodology.

The above discussion applies for realization-by-realization upscaling, in which flow-based upscaling is applied for each geological model. The methods described will be very expensive if applied in this manner for large numbers of models. This motivates the use of ensemble level upscaling (EnLU), where the goal is to provide accurate flow statistics instead of close agreement for each geological realization. Chen and Durlofsky [27] first formulated EnLU for oil-water problems. They considered two-dimensional models with various styles of heterogeneity and fluid mobility ratios. In later work [28], EnLU was extended to challenging three-dimensional well-driven problems, including cases with very high mobility ratios. Upscaling and EnLU procedures for oil-water problems are reviewed in [7]. An approach for upscaling relative permeability using distance-based clustering was presented in [29]. This method is not actually an EnLU approach because it only dealt with

a single realization, though it is conceptually similar to EnLU. The EnLU framework has not yet been applied for compositional problems, as is accomplished in this work.

This paper proceeds as follows. In Section 2, we present the governing equations for oil-gas compositional systems and then describe the global compositional upscaling method. Numerical results using this approach, for a single realization, are presented in Section 3. We then introduce the EnLU methodology for compositional problems in Section 4. Detailed numerical results using EnLU are presented in Section 5. We conclude, in Section 6, with a summary and suggestions for future work.

Full details on the underlying global compositional upscaling procedure, as well as extensive numerical results illustrating its performance and robustness for individual realizations, are presented in [30, 31].

2 Governing equations and global upscaling procedure

In this section, we present the equations governing oil-gas compositional systems. The global upscaling methodology is then described.

2.1 Governing equations

We consider isothermal systems, and assume thermodynamic equilibrium is achieved instantaneously. Capillary pressure, gravitational and diffusive effects are neglected for convenience. The fine-scale mass conservation equation for component i is given by:

$$\nabla \cdot \left(\sum_{j=1}^{n_p} x_{ij}^f \rho_j^f \lambda_j^f \mathbf{k}^f \cdot \nabla p^f \right) - \sum_{j=1}^{n_p} x_{ij}^f \rho_j^f q_j^{w,f} = \frac{\partial}{\partial t} \left(\phi^f \sum_{j=1}^{n_p} x_{ij}^f \rho_j^f S_j^f \right), \quad i = 1,\ n_c, \tag{1}$$

where superscript f indicates a fine-scale variable, x_{ij}^f is the molar fraction of component i in phase j (here j = oil, gas), ρ_j^f is the phase molar density, $\lambda_j^f = k_{rj}^f/\mu_j^f$ is the phase mobility, with k_{rj}^f and μ_j^f the fine-scale relative permeability and viscosity of phase j, $\mathbf{k}^f$ is the (diagonal) permeability tensor, and p^f is pressure. Additional variables are the source/sink term $q_j^{w,f}$, porosity ϕ^f, phase saturation S_j^f, and time t. The total numbers of components and phases are denoted by n_c and n_p ($n_p = 2$ for oil-gas problems). In this work, the fine-scale relative permeabilities are taken to be of the form $k_{rg}^f = (S_g^f)^2$ and $k_{ro}^f = (1 - S_g^f)^2$.

Discretized versions of the mass conservation equation (Eq. 1) are written for each component. These equations are solved in combination with thermodynamic equilibrium constraints of the form $F_{i,o} - F_{i,g} = 0$, where $F_{i,o}$ and $F_{i,g}$ are the fugacities of component i in the oil and gas phases. Other constraints that are introduced to fully specify the system are $S_o^f + S_g^f = 1$ and $\sum_{i=1}^{n_c} x_{ij}^f = 1$.

In this work, we take the coarse-scale equations to be of the same form as the fine-scale equations. Coarse-scale effects are captured by the upscaled parameters/functions $\mathbf{k}^*$ (or T^* and WI^*, described below), λ_j^* (or k_{rj}^*), and α_{ij}. The use of α_{ij} in coarse-scale compositional models was introduced in [21]. Note that we use the superscript $*$ to indicate an upscaled parameter or function (no superscript is used for α_{ij} because it does not have a fine-scale analog), and the superscript c to indicate a coarse-scale dependent variable. Mass conservation for component i is expressed on the coarse scale using:

$$\nabla \cdot \left(\sum_{j=1}^{n_p} x_{ij}^c \alpha_{ij} \rho_j^c \lambda_j^* \mathbf{k}^* \cdot \nabla p^c \right) - \sum_{j=1}^{n_p} x_{ij}^c \alpha_{ij} \rho_j^c q_j^{w,c} = \frac{\partial}{\partial t} \left(\phi^* \sum_{j=1}^{n_p} x_{ij}^c \rho_j^c S_j^c \right), \quad i = 1,\ n_c. \tag{2}$$

Here α_{ij} acts to adjust both the flux term and the well term for each component in each phase. The constraints specified above also appear. Coarse-scale porosity ϕ^* is computed such that pore volume is preserved between the coarse block and the corresponding fine-scale cells.

2.2 Global compositional upscaling procedure

The techniques applied here entail calculation of coarse-scale parameters with the goal of matching fluxes, between fine and coarse solutions, through block interfaces (or well completions). We proceed by first computing the upscaled transmissibility T^* and well index WI^* from a global single-phase flow solution. We then solve the global compositional problem, and use this solution to compute the upscaled relative permeability functions k_{rj}^*, which capture phase flow rates in the coarse-scale model, and α_{ij}, which capture component flow rates in each phase. To improve the accuracy of the overall procedure, we iterate on the α_{ij}, using an approach analogous to those applied in [3, 4] for the calculation of T^*. We now present expressions for the upscaled parameters. For full details, see [30, 31].

Figure 1 shows the fine- and coarse-scale simulation grids for both the global and local regions. The first step

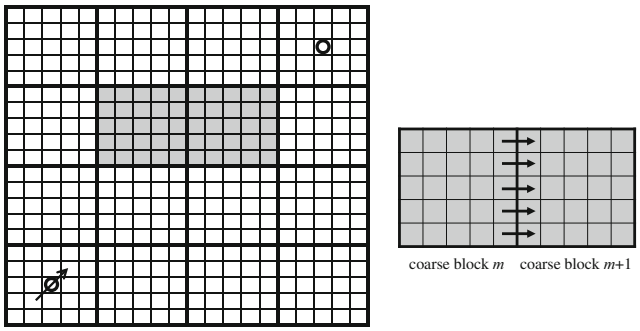

(a) global domain (b) local region

Fig. 1 Schematic showing the global domain (with one injection well and one production well) and a local two-coarse-block region (*light lines* indicate the fine grid and *heavy lines* indicate the coarse grid)

of the upscaling methodology is to solve the global steady-state incompressible single-phase pressure equation (with viscosity $\mu = 1$), with flow driven by the actual wells in the target problem (Fig. 1a). In the calculation of upscaled transmissibility, our aim is to compute T^* such that the integrated (summed) fine-scale flux through the region corresponding to the target coarse interface is reproduced in the coarse-scale solution. By approximating the coarse quantities as averages/sums over the corresponding fine-scale regions, T^* can be calculated as:

$$T^* = \frac{\sum_l (q^f)_l}{\langle p^f \rangle_m - \langle p^f \rangle_{m+1}}, \tag{3}$$

where $\langle \cdot \rangle_m$ denotes a bulk-volume-average (for pressure) or pore-volume-average (for other quantities) property computed over the fine-scale cells lying within coarse-block m (see Fig. 1b), $\sum_l (q^f)_l$ is the integrated fine-scale flux through the target coarse interface, with l denoting the fine-scale interfaces that lie on the target coarse interface (designated by arrows in Fig. 1b). The computation for the upscaled well index WI^* is similar to that for T^*. Specifically, we now apply:

$$WI^* = \frac{\sum_l (q^{w,f})_l}{\langle p^f \rangle_m - \langle p^{w,f} \rangle_m}, \tag{4}$$

where $(q^{w,f})_l$ is the flow rate between the well and fine-scale cell l (with l designating a cell that lies within coarse-well-block m) and $\langle p^{w,f} \rangle_m$ is the average wellbore pressure over coarse-well-block m.

To compute $k^*_{rj}(S^c_j)$ and $\alpha_{ij}(S^c_j)$, we solve the global compositional flow problem. This is by far the most time-consuming step of the procedure. The upscaled relative permeabilities are determined such that the integrated fine-scale flux of each phase ($\sum_l (q^f_j)_l$) is captured in the coarse-scale model. This results in the following expression for k^*_{rj}:

$$k^*_{rj}(S^c_j) = \frac{\langle \mu^f_j \rangle \sum_l \left(q^f_j\right)_l}{T^* \langle \rho^f_j \rangle \left(\langle p^f \rangle_m - \langle p^f \rangle_{m+1} \right)}. \tag{5}$$

The average fine-scale quantities $\langle \mu^f_j \rangle$, $\langle \rho^f_j \rangle$ and $S^c_j = \langle S^f_j \rangle$ are computed as pore-volume-averages over the fine-scale cells lying within the upstream coarse block.

In this work, α_{ij} are taken to be functions of S^c_j in the upstream block. These functions are computed such that the integrated fine-scale flux of each component in each phase, given by $\sum_l (q^f_{ij})_l$, is preserved in the coarse model. By approximating x^c_{ij} in terms of a pore-volume average over the upstream block, we have:

$$\alpha_{ij}(S^c_j) = \frac{\langle \mu^f_j \rangle \sum_l \left(q^f_{ij}\right)_l}{T^* k^*_{rj}(S^c_j) \langle \rho^f_j \rangle \langle x^f_{ij} \rangle \left(\langle p^f \rangle_m - \langle p^f \rangle_{m+1} \right)}. \tag{6}$$

Consistent with the findings in [15–17], upscaled k^*_{rj} and α_{ij} are also required for the coarse-scale well model. These functions are computed using expressions similar to Eqs. 5 and 6, except $(q^{w,f}_j)_l$ and $(q^{w,f}_{ij})_l$ appear in place of $(q^f_j)_l$ and $(q^f_{ij})_l$, and the pressure difference is between the wellbore and the coarse well block (as in Eq. 4). See [30, 31] for the detailed expressions for coarse-scale well terms.

The upscaled k^*_{rj} and α_{ij} computed using Eqs. 5 and 6 may, in some cases, display unphysical behavior. This often results from having small (phase or component) flow rates, along with small pressure differences, through a particular coarse interface. In this work, we treat as 'unphysical' any k^*_{rj} or α_{ij} values that are less than zero or larger than five. These values are eliminated from the upscaled functions. Further discussion regarding the causes of these unphysical points, and our detailed treatments, are provided in [30].

We have found that enhanced accuracy can be achieved by iterating on α_{ij} to minimize the difference between fine- and coarse-scale fluxes. This type of treatment was introduced in [3] to improve the accuracy of T^* in a global single-phase upscaling procedure. With this approach, at a particular time step, the next iterate of α_{ij}, denoted $\alpha^{\nu+1}_{ij}$, is given by

$$\alpha^{\nu+1}_{ij} = d\alpha^{\nu}_{ij} + (1-d)\frac{\sum_l \left(q^f_{ij}\right)_l}{q^{c,\nu}_{ij}}\alpha^{\nu}_{ij}. \tag{7}$$

Here α^{ν}_{ij} is the α_{ij} value at the current iteration, q^c_{ij} is the coarse-scale flux of component i in phase j through

the target interface, $\sum_l (q_{ij}^f)_l$ is the integrated fine-scale flux, and d is a damping factor (we use $d = 0.7$). This procedure requires us to repeat the time step within the coarse-scale simulation several times (we typically use five iterations), though this is very inexpensive compared to the global compositional solution. In this work, Stanford's General Purpose Research Simulator, GPRS [32, 33], is applied for all fine- and coarse-scale simulations. We modified this code to enable iteration on α_{ij} as defined in Eq. 7.

3 Numerical results using global upscaling procedure

We now demonstrate the global compositional upscaling procedure for a single realization of a heterogeneous two-dimensional $(x - y)$ model. The isotropic $(k_x = k_y)$ permeability field was generated using sequential Gaussian simulation [34] with a spherical variogram model and dimensionless correlation lengths of $l_x = l_y = 0.3$. The variance of log-permeability, designated σ, was set to 1.8. This corresponds to a relatively high degree of heterogeneity. The fine-scale grid contains 99×99 cells, of dimensions $\Delta x = \Delta y = 25$ ft and $\Delta z = 10$ ft. The model contains four production wells and one injection well arranged in a five-spot pattern. The permeability field and well locations are shown in Fig. 2. For this case, porosity is related to permeability via $\phi = 0.02 \log k + 0.136$, with minimum and maximum porosity values constrained to be 0.15 and 0.25.

The injection well is prescribed to operate at a fixed pressure of 1500 psi and the production wells all operate at 500 psi. Initial reservoir pressure is 800 psi. Temperature is fixed at 300 K (the problem is isothermal). The initial oil is a mixture of four components: C_1 (10 %), CO_2 (18.09 %), C_4 (37.66 %), and C_{10} (34.25 %). Pure C_1 is injected. This

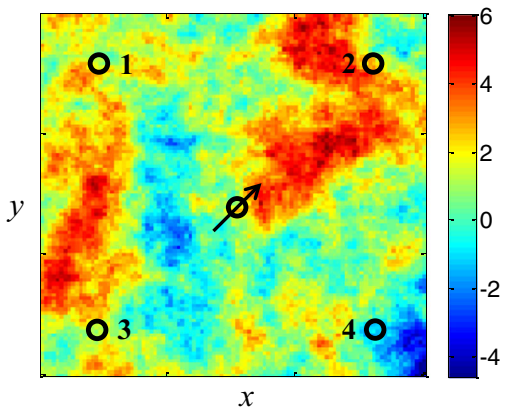

Fig. 2 Permeability field ($\log k$) and well locations

set of components was considered in [35] and corresponds to an immiscible system.

The coarse-scale model is constructed by uniformly coarsening the fine model by a factor of nine in each direction (for an upscaling ratio of 81). The coarse model thus contains $11 \times 11 = 121$ blocks. We simulate flow for a period of 2500 days. As noted earlier, GPRS is used for all simulations.

Figure 3 displays the field oil and gas production rates (i.e., summed over the four producers) for this case. Results are shown for the fine-scale model (black curve), the 'standard' coarse model (red dashed curve), which was generated by computing T^* and WI^* and using $k_{rj}^* = k_{rj}^f$ and $\alpha_{ij} = 1$, a globally upscaled model generated with α_{ij} iteration (green points), a globally upscaled model generated without iterating on α_{ij} (blue dot-dashed curve), and a coarse model generated using only global two-phase upscaling (pink dot-dashed curve). This last model includes T^*, WI^*, and k_{rj}^*, but not α_{ij} (which means $\alpha_{ij} = 1$). Results for these different models allow us to assess the impact of the various upscaled quantities. We reiterate that, in all coarse models, T^* and WI^* are computed using global single-phase upscaling.

We see that the standard coarse model leads to significant errors relative to the reference fine-scale solution. For example, the gas rate is consistently underpredicted by the standard coarse model, and the peak in oil rate occurs about 600 days late. Global two-phase upscaling provides results that are generally accurate, though error relative to the fine-scale model is still evident (e.g., in the time of peak oil production). The use of upscaled α_{ij} (globally upscaled model without iteration) improves the results further relative to the global two-phase upscaling model. The iterative global upscaling model provides the best overall accuracy, including the precise prediction of peak oil production rate and time. The results in Fig. 3 clearly show the added benefit, in terms of solution accuracy, of each component of the upscaling procedure.

We next present, in Fig. 4, the field production rates for all four components. Because pure C_1 is injected in this case, the C_1 production rate increases dramatically after breakthrough, which occurs at around 400 days in the fine-scale model. Most of the C_4 and C_{10} stays in the oil phase, so their production rates (Fig. 4c, d) are similar to the oil production rate in Fig. 3a. Comparisons of fine- and coarse-scale results lead to observations that are analogous to those offered above, namely that the use of the standard coarse model leads to inaccurate results, and that the already high accuracy of the non-iterated globally upscaled model is improved through iteration. Interestingly, we observe more significant error in CO_2 rates when using global two-phase upscaling only. This is because the partitioning of CO_2 between the gas and oil phases is strongly

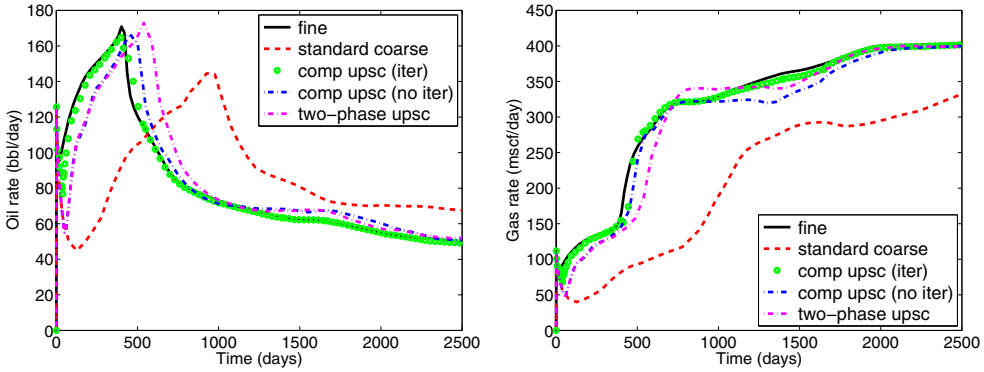

(a) Oil rate (b) Gas rate

Fig. 3 Oil and gas field production rates for single-realization example

impacted by phase behavior, and this is not fully captured in the coarse-scale model unless we include α_{ij}. These results demonstrate that our compositional upscaling procedure is able to capture component flow rates in addition to phase flow rates. Well-by-well production results, though not shown here, also display high accuracy.

Finally, in Fig. 5, we show the pressure fields at 2500 days for some of the models. The averaged fine-scale result (Fig. 5b) is obtained by bulk-volume-averaging the fine-scale pressure field (Fig. 5a) onto the coarse grid. We see the impact of the low permeability regions between the injector and Producers 1 and 3 in the pressure distributions. Significant discrepancy between the standard coarse model result (Fig. 5c) and the averaged fine-scale field is evident. The globally upscaled model (Fig. 5d), by contrast, provides a very accurate pressure distribution, and the improvement relative to the standard coarse model is significant.

For additional single-realization upscaling results, including phase and component production rates for individual wells, robustness results, and three-dimensional model results, see [30, 31].

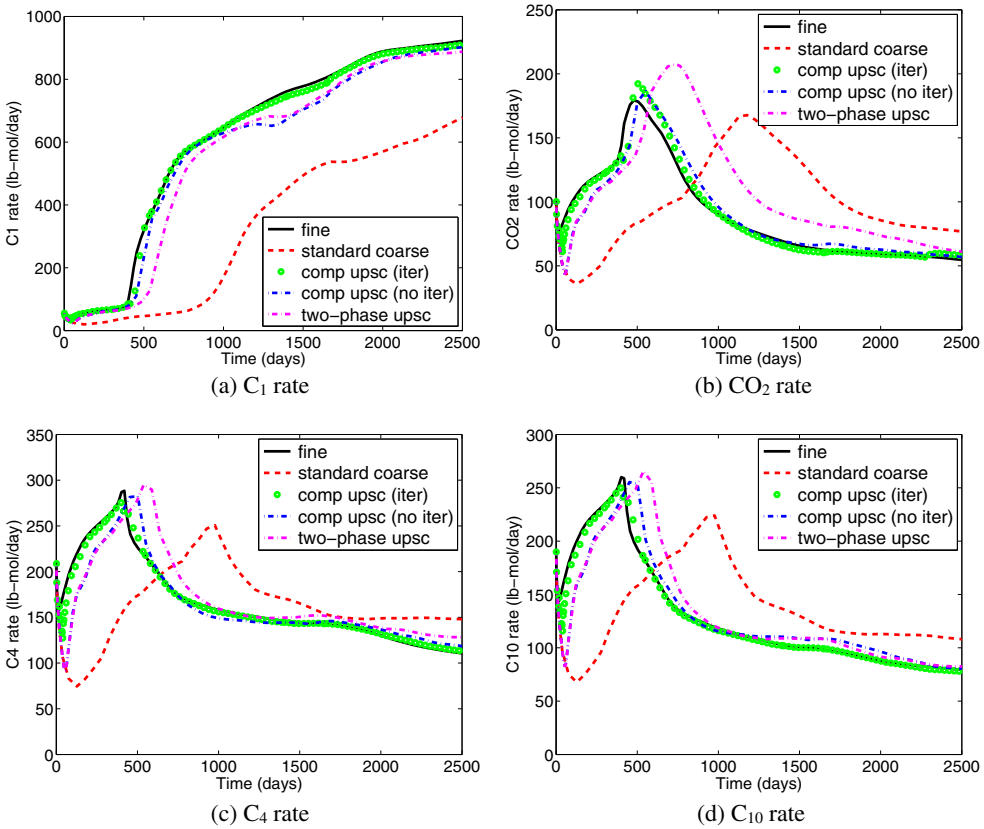

(a) C_1 rate (b) CO_2 rate

(c) C_4 rate (d) C_{10} rate

Fig. 4 Component field production rates for single-realization example

4 Ensemble level upscaling methodology

As discussed in Section 1, ensemble level upscaling is applicable when the goal is to simulate multiple geological realizations. In EnLU, full flow-based compositional upscaling, as described in the previous section, is applied only to a small fraction of the realizations, though global transmissibility upscaling is performed for all realizations. The k^*_{rj} and α_{ij} coarse-scale functions are then 'calibrated' with easily-computed attributes, which can be based on either (static) local permeability data or single-phase flow quantities generated during single-phase upscaling. Upscaled functions for all interfaces in new realizations are then statistically generated based on the calibrations and the spatial correlation structure in the upscaled functions, as observed in models for which full flow-based compositional upscaling was applied. We now describe the detailed EnLU procedure.

4.1 Parameterization of k^*_{rj} and α_{ij}

As noted earlier, the upscaled quantities k^*_{rj} and α_{ij} are here taken to be functions of S^c_g only. Two k^*_{rj} curves for the example presented in Section 3, along with the fine-scale (rock) curves, are shown in Fig. 6. The upscaled curves differ due to the different permeability and flow fields experienced by the two interfaces. We now introduce a parameterization for the coarse-scale functions, which acts to facilitate their calibration to quickly-computed attributes.

In this work, k^*_{rj} and α_{ij} are represented in terms of two quantities, designated δk_{rj} and $\delta\alpha_{ij}$, that measure the (signed) difference between the upscaled and fine-scale curves. These differences are computed as follows:

$$\begin{aligned}\delta k_{rj} &= \frac{1}{N}\sum_{i=1}^{N}\left(k^*_{rj}(S_{g,i}) - k^f_{rj}(S_{g,i})\right),\\ \delta\alpha_{ij} &= \frac{1}{N}\sum_{i=1}^{N}\left(\alpha_{ij}(S_{g,i}) - 1\right),\end{aligned} \tag{8}$$

where the N saturation values are equally spaced between 0 and 1, and $S_{g,i}$ indicates S_g at point i. Because $\alpha_{ij} = 1$ in the fine-scale model, $(\alpha_{ij} - 1)$ is used in the calculation of $\delta\alpha_{ij}$.

We note that absolute values were applied in the parameterizations in [27, 28]. Because we observe both positive and negative δk_{rj} in our global upscaling results (i.e., some of the k^*_{rj} curves are on average above, and some are on average below, the k^f_{rj} curve), we instead apply the form shown in Eq. 8. If absolute values were used in place of

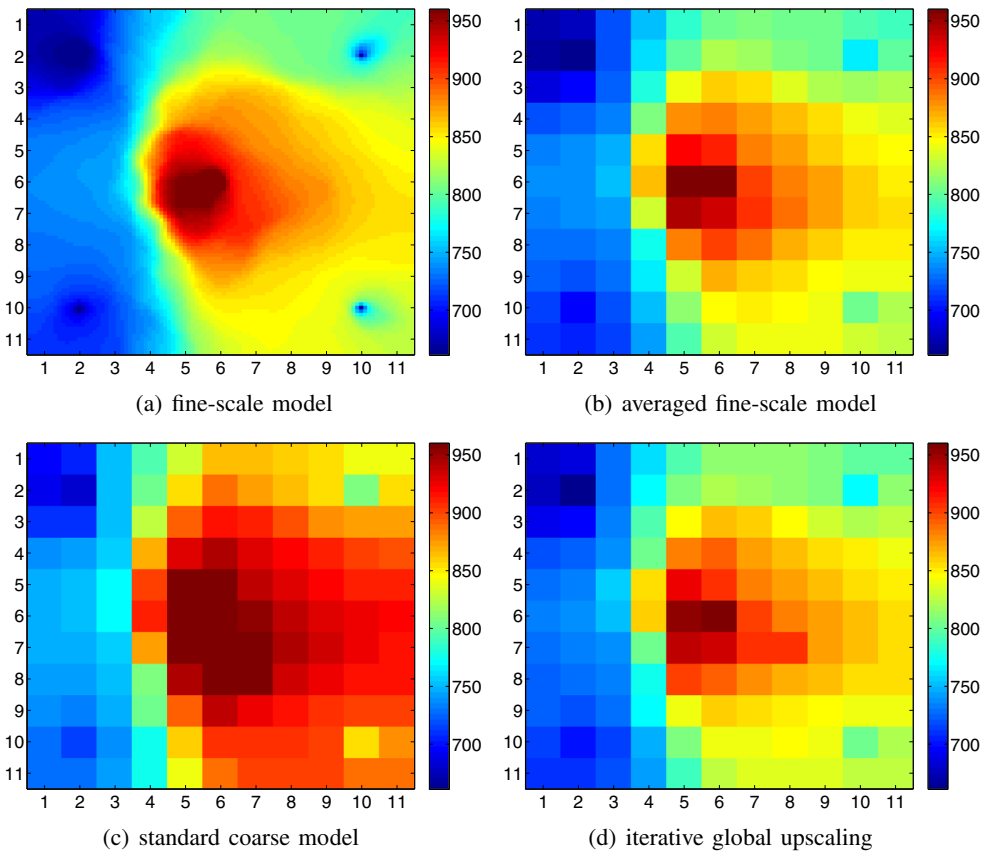

(a) fine-scale model (b) averaged fine-scale model

(c) standard coarse model (d) iterative global upscaling

Fig. 5 Pressure distributions for single-realization example

signed differences, we would be unable to distinguish negative deviations from positive deviations, which would affect model accuracy. As is evident in Fig. 6, the sign of the difference between k^*_{rj} and k^f_{rj} can change over the range of S^c_g, and this results in some amount of cancellation in the δk_{rj} computation in Eq. 8. Over most of the S^c_g range, however, k^*_{rj} is generally either above or below k^f_{rj}, so the cancellation effect is typically small. Thus, it is still advantageous to use a signed difference in Eq. 8 rather than the absolute value.

Because of the variable (and sometimes irregular) shape of some of the upscaled functions, this parameterization cannot differentiate upscaled functions very precisely (e.g., different k^*_{rj} curves may correspond to the same or very similar δk_{rj} values). Other methods have been proposed for representing upscaled relative permeability (or total mobility and fractional flow) functions, and some of these are discussed within the context of EnLU in [27]. Dupouy et al. [36], for example, suggested several approaches including the use of functional models to represent the upscaled curves. None of the proposed methods is fully general, however, given the range of behaviors the upscaled functions can display. The simple parameterization used here has the advantage of requiring us to calibrate, and then determine, only a single parameter for each upscaled function within EnLU. Were we to represent coarse-scale functions in terms of several parameters, we would then need to calibrate and determine multiple (potentially related) parameters, which could lead to additional complications. In any event, the use of Eq. 8 will be shown to be fully adequate for current purposes, as the goal in EnLU is to match fine-scale flow statistics rather than to achieve realization-by-realization agreement.

4.2 Calibration of k^*_{rj} and α_{ij} to attributes

We now define attributes that (1) can be quickly calculated for a given coarse-scale interface, and (2) are able to provide a reasonable correlation with δk_{rj} or $\delta\alpha_{ij}$. For new realizations, we can then simply compute the attributes and apply the previously established correlation to provide the upscaled functions. This approach avoids the need for any additional (expensive) flow-based upscaling.

In general, the appropriate attributes for a particular application may be somewhat problem-specific, and their determination requires numerical experimentation. In this work, however, we found that the attributes suggested in earlier EnLU studies provided satisfactory performance. The specific set of attributes used here are the standard deviation of the fine-scale log-permeability over the upstream coarse block ($\sigma = \sigma(\log k)$), the coefficient of variation of the fine-scale single-phase velocity ($C = \mathrm{CV}(u^f)$) computed for the upstream coarse block, and the integrated fine-scale single-phase flow rate ($Q = \sum q^f$) through the target coarse interface.

The attribute σ can be computed quickly from the fine-scale permeability distribution, and C and Q can be readily calculated from the global fine-scale pressure solution used to determine T^* and WI^* in global single-phase upscaling. Previous work [37] on subgrid modeling for two-phase flow problems showed that upscaled relative permeability functions are impacted significantly by fluctuations (relative to the block average) of fine-scale saturation and velocity within the coarse grid block. These effects are captured approximately by the attributes σ (which quantifies local permeability heterogeneity) and C (which describes the variation of the fine-scale velocity). In addition, we observed that the upscaled functions correlate with the integrated fine-scale single-phase flow rate Q. This parameter is able to distinguish interfaces or well blocks subject to different types of flow conditions, which is useful for assigning upscaled functions. The upscaled (parameterized) functions can now be expressed as:

$$\delta k_{rj} = \mathcal{F}_1(\sigma, \mathrm{C}, Q), \quad \delta\alpha_{ij} = \mathcal{F}_2(\sigma, \mathrm{C}, Q). \tag{9}$$

The calibration used in this work differs from that used in [27, 28]. In those studies, the attributes were clustered (using K-means clustering) and the cumulative distribution

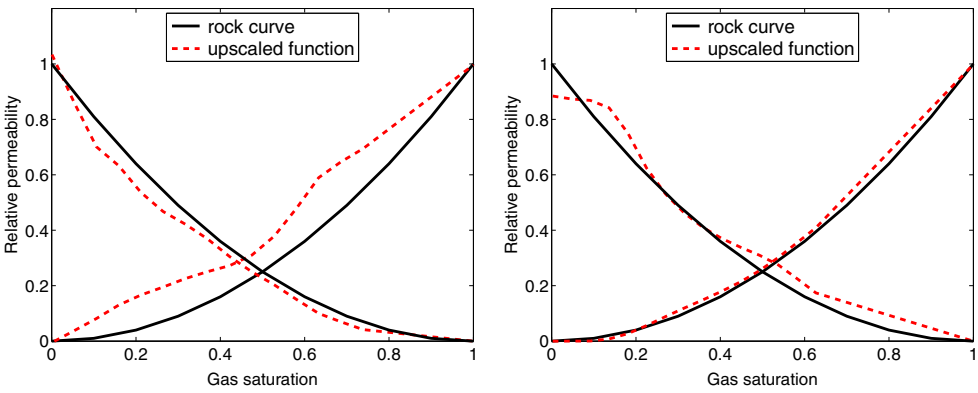

Fig. 6 Upscaled (k^*_{rj}) functions for two different coarse interfaces for the example case in Section 3

function (CDF) for each cluster was constructed. The CDFs were then used to provide a statistical correlation between the upscaled functions and the attributes. In this work, we establish the correlation directly using Eq. 9. For interfaces for which the upscaled functions have been computed through flow simulation, we first normalize (using uniform score transformation [38]) the attributes so they range from 0 to 1. We can (conceptually) then plot each set of attributes in normalized $\sigma - C - Q$ space. Each of these points corresponds to a particular δk_{rj} and $\delta\alpha_{ij}$. Given a new set of attributes (normalized $\sigma - C - Q$ values), we can then apply some type of interpolation, or simply find the 'closest' calibration point, to determine δk_{rj} and $\delta\alpha_{ij}$.

For the two-dimensional models considered in this work, we perform this calibration separately for interfaces oriented in the x- and y-directions. Interfaces surrounding the well blocks are also treated separately, as are the upscaled functions for the production and injection well blocks (recall that these upscaled functions appear in the well model). For three-dimensional systems, we would additionally treat z-direction interfaces separately. This approach should render the overall EnLU procedure applicable for anisotropic systems, in which case δk_{rj} and $\delta\alpha_{ij}$ may vary strongly with direction. Although not considered here, we note that EnLU was successfully applied to three-dimensional anisotropic oil-water systems (with $k_z/k_x = 0.1$) in [28]. In addition, the underlying global compositional upscaling procedure has been applied for anisotropic three-dimensional systems in [30]. Thus, we expect the compositional EnLU procedure presented here to be applicable for such systems, though this will have to be verified in future work.

4.3 Estimation of upscaled functions for new realizations

For new realizations, in order to avoid performing flow-based upscaling, we simply compute normalized σ, C and Q for a target interface, and then find the closest (in terms of Euclidean distance) calibration point in normalized $\sigma - C - Q$ space. The δk_{rj} and $\delta\alpha_{ij}$ values associated with the closest calibration point can then be assigned to the target interface. As indicated above, different calibrations are used for different types of interfaces.

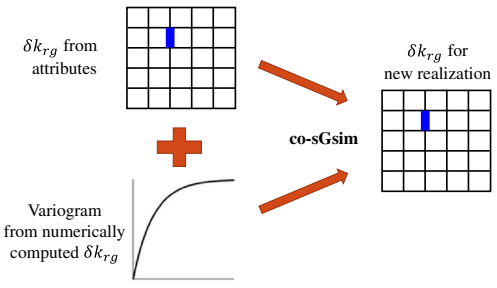

Fig. 7 Schematic of the geostatistical procedure used to assign δk_{rg}

Were we to use directly the δk_{rj} and $\delta\alpha_{ij}$ computed in this manner, the assignment of upscaled functions would be deterministic. In addition, the functions might not honor the spatial correlation structure observed in the calibration data. It may in fact be important to honor, at least approximately, the spatial correlation structure of δk_{rj} and $\delta\alpha_{ij}$, because this structure can impact flow behavior (e.g., gas flow rate will be enhanced through a region with continuously high δk_{rg} values). The deterministically generated δk_{rj} and $\delta\alpha_{ij}$ somewhat honor the spatial structure of the calibration data, since the attributes follow, to some extent, these spatial statistics. We have observed, however, that the correlation structure of δk_{rj} and $\delta\alpha_{ij}$ is better resolved through application of a geostatistical procedure, which we now describe.

This issue was addressed in [28], and we proceed here along similar lines. We focus here on δk_{rg} (assignment of other upscaled functions will be described below). To assign δk_{rg}, we apply sequential Gaussian co-simulation (co-sGsim) to combine the δk_{rg} determined from Eq. 9 with estimates that honor the spatial correlation structure observed in the δk_{rg} generated from global compositional upscaling (the calibration data). To accomplish this, variogram modeling is performed after the requisite number of realizations have been upscaled using the flow-based procedure. All of the calibration data for a particular type of interface are used in the variogram modeling. We then treat the δk_{rg} determined from Eq. 9 as 'soft' data. In co-sGsim, these soft data are combined with values estimated from the variogram to provide the final δk_{rg}. This procedure is illustrated schematically in Fig. 7.

When applying co-sGsim, to alleviate the impact of extreme values, we first perform a uniform score transformation [38] of δk_{rg}. Geostatistically simulated values must then be back-transformed to obtain the final δk_{rg}. Because δk_{rg} is just a single parameter, we require a means to proceed from δk_{rg} to $k^*_{rg}(S^c_g)$ (and similarly for k^*_{ro} and α_{ij}). Our approach is as follows. Given a co-sGsim value of δk_{rg} for a target interface, we first find the closest calibration δk_{rg} value. Then, the $k^*_{rg}(S^c_g)$ curve that corresponds to this δk_{rg} value is assigned to the target interface. We additionally assign the corresponding calibration $k^*_{ro}(S^c_g)$ and $\alpha_{ij}(S^c_g)$ functions to the target interface; i.e., the k^*_{ro} and α_{ij} associated with the same coarse interface as k^*_{rg}. This treatment acts to maintain consistency between the coarse-scale functions, in that they all derive from the same coarse-scale interface. The assignment is based on δk_{rg} because we have found this parameter to display the clearest spatial correlation structure.

We note that a small change in the δk_{rg} value can result in the selection of a different set of upscaled functions. We

expect the upscaled functions associated with nearby δk_{rg} to be sufficiently similar, however, such that this treatment will not introduce significant inaccuracy. Based on the numerical results presented below, this procedure does appear to provide accurate ensemble level predictions. It is possible that an alternative approach for proceeding from δk_{rg} to a set of upscaled functions could lead to even better accuracy, either at the ensemble or realization-by-realization level.

The assignment of k^*_{rj} and α_{ij} for well terms is based only on attributes and does not require co-sGsim. We proceed in this way because the wells are independent of each other, so there is no spatial correlation structure to exploit. For additional technical details on the assignment of upscaled functions in EnLU, see [30].

5 Numerical results for EnLU

We now apply EnLU for uncertainty quantification for two different systems. The first case involves Gaussian models, as considered in Section 3, and the second case entails channelized models. Five-spot well patterns are used in both cases.

A total of 100 realizations are employed in each case. We first perform fine-scale simulation for all 100 realizations to provide reference results (this is the step we seek to avoid in practice). Full flow-based upscaling (global compositional upscaling, with iteration) is then performed for all realizations. We view these upscaled results as (essentially) the best coarse-scale results that we can achieve, so in this sense they represent the reference to which EnLU should be compared. In the EnLU results, calibration data are generated by performing flow-based upscaling on 10 of the 100 realizations, except where otherwise noted. The realizations used for flow-based upscaling are those with the largest injection/production rates, as determined during the transmissibility upscaling step. We select these realizations because larger flow rates generally result in more regions of the model experiencing a significant range of variation in S^c_g, and this improves the quality of the upscaled functions used in EnLU.

5.1 Gaussian permeability field

As in Section 3, the fine-scale model contains 99×99 grid blocks and the coarse-scale model is uniformly upscaled to 11×11. The geostatistical parameters, fluid system, initial conditions, and well specifications are as described previously (pure C_1 is injected into a four-component system). The only property that is different is porosity; here we use a constant value of 0.2. Three permeability ($\log k$) realizations are shown in Fig. 8. These realizations are not conditioned to any well data, so the permeability fields differ significantly.

Fine-scale simulation results for oil and gas field production rates for all 100 realizations are shown in Fig. 9. The thin gray lines represent results for each realization, and the heavy lines indicate the P10 (lower dashed curves), P50 (solid curves), and P90 (upper dashed curves) flow statistics. Substantial realization-to-realization variation in both oil and gas production rates is evident. Note that the ratio of the P90 gas rate to the P10 gas rate at 3000 days is over a factor of 10.

We now compare the flow statistics for coarse-scale models to those from the fine-scale models. Figure 10 presents the P10, P50, and P90 curves for field oil production rate. In Fig. 10 and subsequent figures, the solid line indicates the P50 production rate and the dashed lines indicate the P10 and P90 production rates. Fine-scale results are shown in black in all figures. Results using standard coarse models, which again involve the use of T^* and WI^* but no other upscaled quantities, are shown as the red curves in Fig. 10a. These models do not provide very accurate predictions, and they clearly underpredict oil rate at early time. Results using flow-based upscaling for all 100 models are shown as the green curves in Fig. 10b. These results closely match the fine-scale results, as would be expected. EnLU results, shown as the blue curves in Fig. 10c, are also seen to be of clearly acceptable accuracy. They are not as accurate as the results in Fig. 10b, but they provide significant improvement relative to the standard coarse results shown in Fig. 10a. This is significant, since these results were generated by performing global upscaling on only 10 % of the models.

Results for field gas production rate and component C_1 production rate are presented in Figs. 11 and 12. The standard coarse models (Figs. 11a and 12a) significantly underpredict both quantities, while the globally upscaled and EnLU-generated models provide generally high degrees of accuracy. A slight degradation in EnLU accuracy is seen in the P90 results for C_1 production rate (Fig. 12c).

We next present results for a particular (representative) well, Producer 1. The P10, P50, and P90 gas rates for Producer 1 are shown in Fig. 13. Consistent with Fig. 11, we again observe large errors in results using standard coarse models, while globally upscaled models and EnLU models provide generally accurate results. The EnLU results are not as accurate as those for field rates (compare Figs. 11c to 13c), though they are clearly of acceptable accuracy.

Finally, we present realization-by-realization results for the error incurred by the different approaches. Error in phase

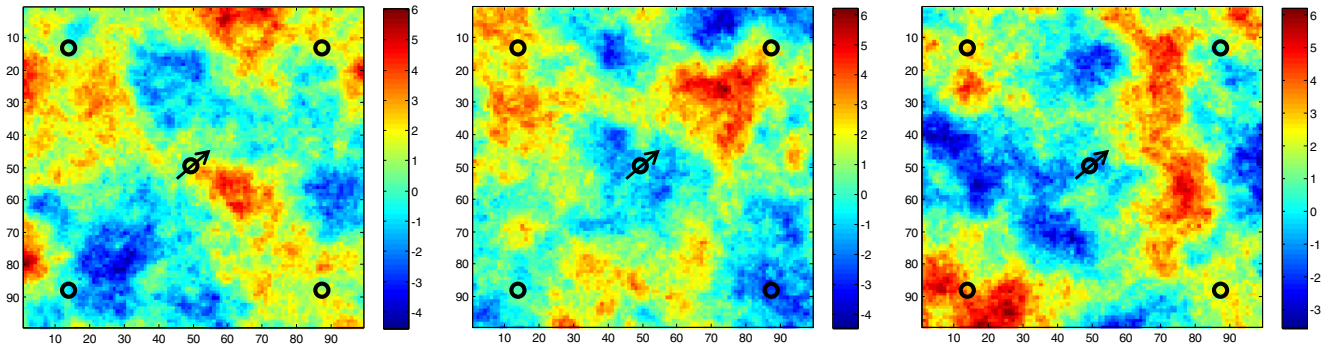

Fig. 8 Permeability maps ($\log k$) for three realizations (Gaussian permeability field)

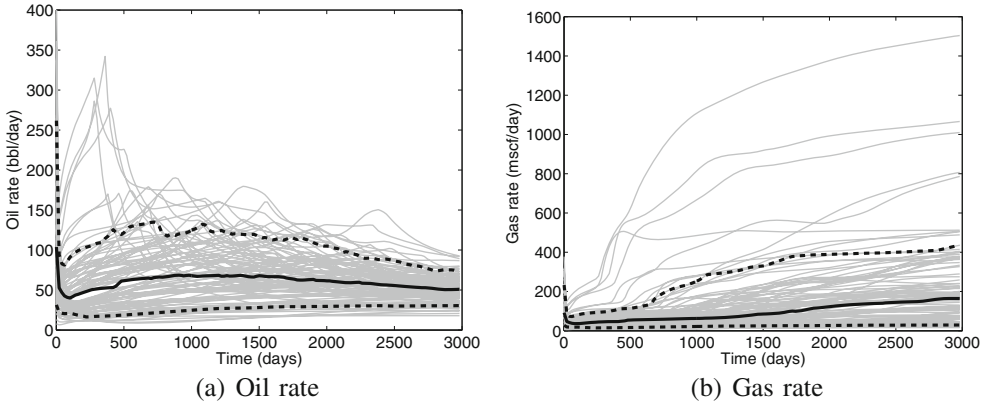

(a) Oil rate (b) Gas rate

Fig. 9 Oil and gas field production rates for 100 fine-scale models (Gaussian permeability field). P10, P50, and P90 results shown as heavy lines

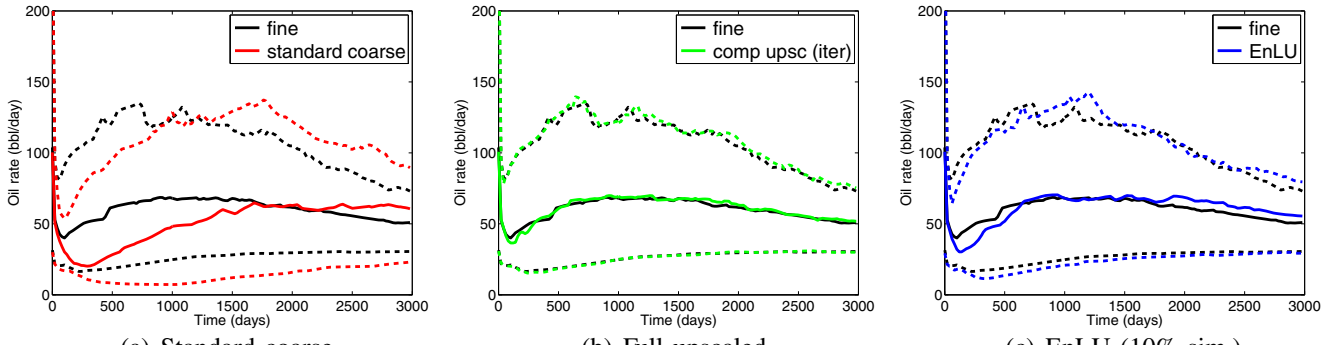

(a) Standard coarse (b) Full upscaled (c) EnLU (10% sim.)

Fig. 10 P10, P50, and P90 curves for oil field production rate (Gaussian permeability field)

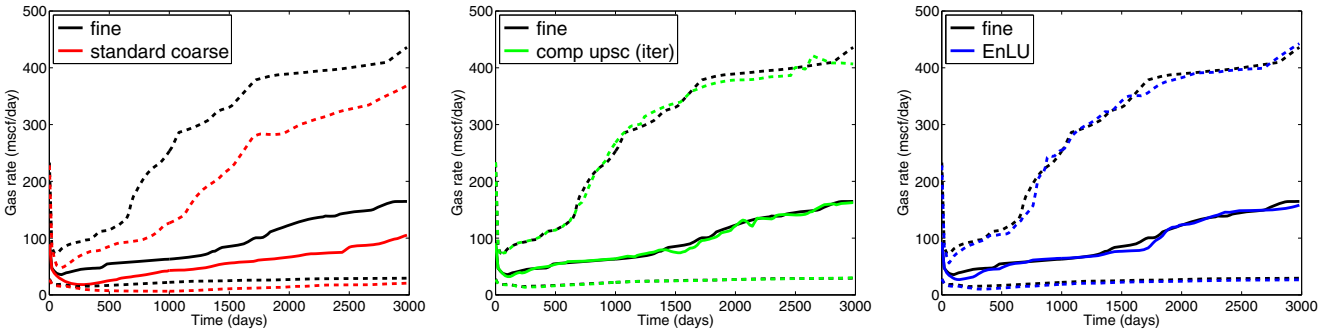

(a) Standard coarse (b) Full upscaled (c) EnLU (10% sim.)

Fig. 11 P10, P50 and P90 curves for gas field production rate (Gaussian permeability field)

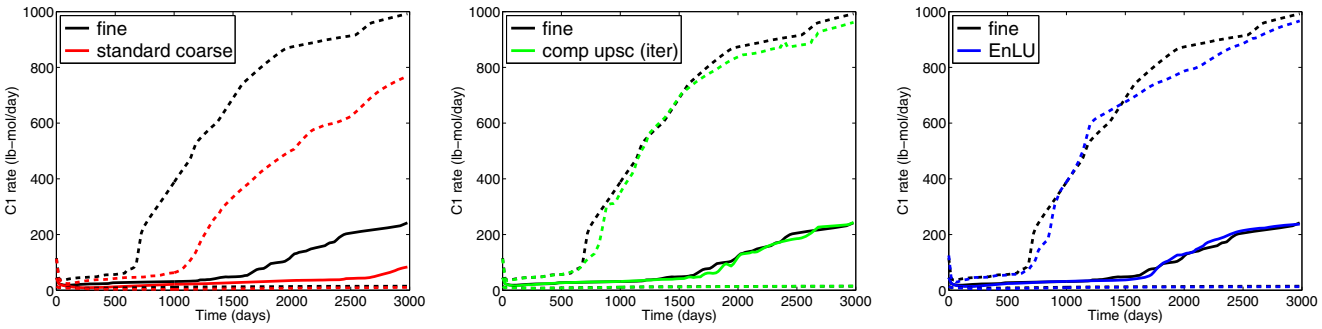

(a) Standard coarse (b) Full upscaled (c) EnLU (10% sim.)

Fig. 12 P10, P50, and P90 curves for C_1 field production rate (Gaussian permeability field)

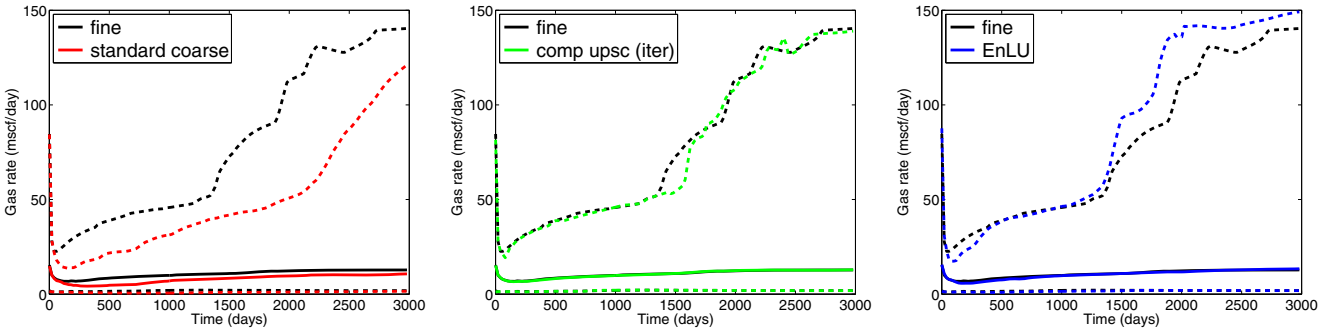

(a) Standard coarse (b) Full upscaled (c) EnLU (10% sim.)

Fig. 13 P10, P50, and P90 curves for gas production rate for Producer 1 (Gaussian permeability field)

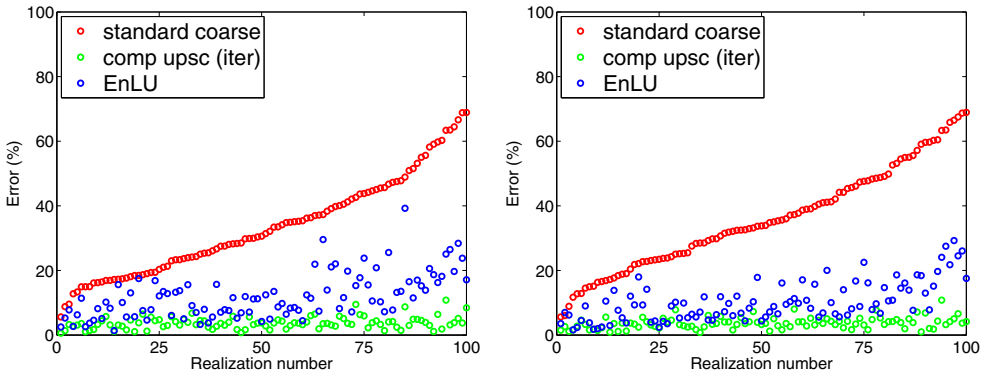

Fig. 14 Relative error in oil and gas field production rates for 100 realizations (Gaussian permeability field)

Table 1 Median errors for oil, gas, and all component field production rates

Coarse model	Oil	Gas	C_1	CO_2	C_4	C_{10}
Standard coarse	31.2 %	33.8 %	49.8 %	35.2 %	28.7 %	30.6 %
Full global upscaling	3.3 %	3.1 %	4.3 %	4.4 %	3.2 %	3.5 %
EnLU	11.1 %	9.3 %	13.6 %	12.4 %	8.5 %	10.6 %

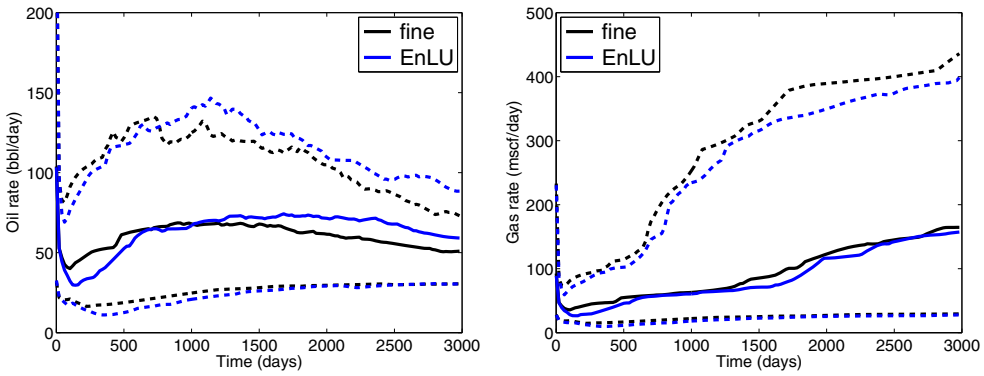

Fig. 15 P10, P50, and P90 curves for oil and gas field production rates (Gaussian permeability field). EnLU results use flow-based upscaling of only five realizations (previous results used ten realizations)

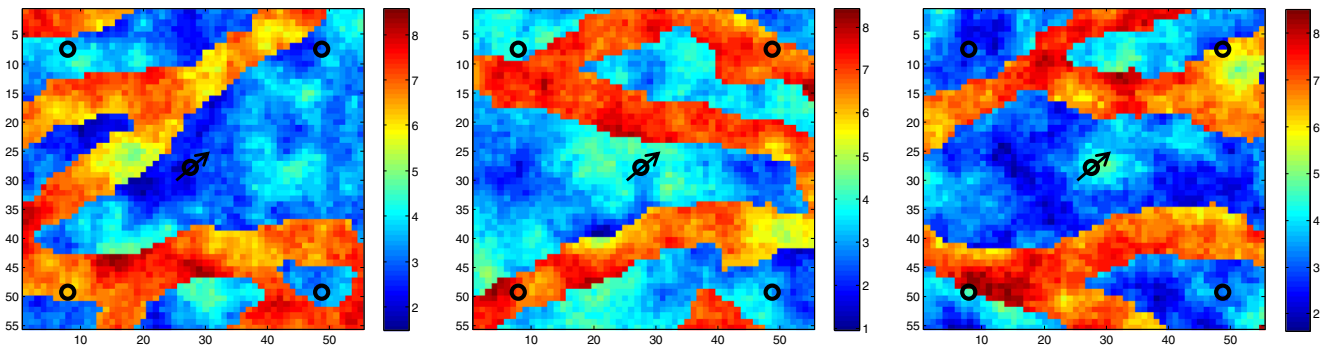

Fig. 16 Permeability maps ($\log k$) for three realizations (channelized permeability field)

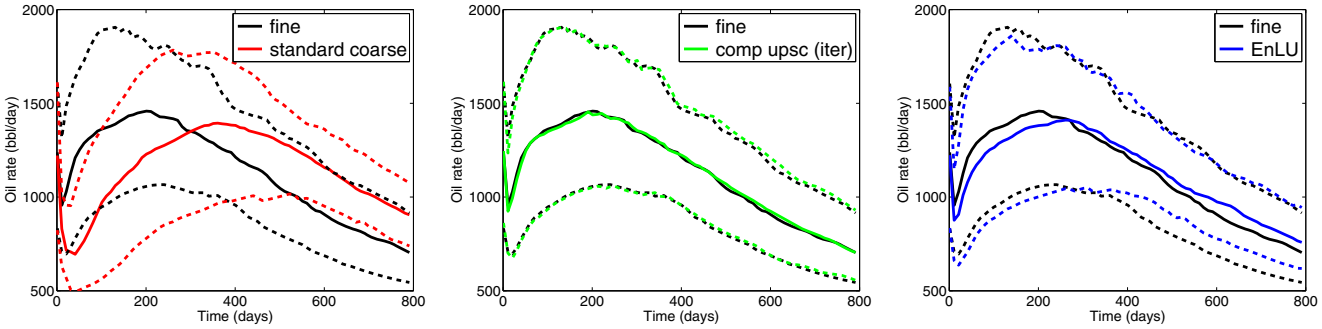

(a) Standard coarse (b) Full upscaled (c) EnLU (10% sim.)

Fig. 17 P10, P50, and P90 curves for oil field production rate (channelized permeability field)

production rate, designated E_j, is computed as:

$$E_j = \frac{\int_t \left| q_j^c - q_j^f \right| dt}{\int_t q_j^f \, dt}, \tag{10}$$

where q_j^c and q_j^f are coarse- and fine-scale field production rates for phase j. An analogous expression is used to compute error in component rates. The realizations in Fig. 14 are ordered based on the error in the standard coarse model (indicated by the red points). The ordering differs between Figs. 14a and b. The median errors for field oil, gas, and all component production rates, for each method, are listed in Table 1. For oil rate, the median error in the standard coarse models is over 30 %. Full global upscaling reduces the median error to about 3 %, while EnLU provides a median error of 11 %.

For all of the entries in Table 1, EnLU errors are between those for full global upscaling and standard coarsening, though they are much closer to those for full global upscaling. These results are consistent with expectations. Although EnLU is more accurate than standard upscaling, it does not provide results that are as accurate as those achieved by performing flow-based upscaling for all realizations. Another advantage of EnLU over standard upscaling is that EnLU error is largely unbiased, which enables accurate predictions for P10, P50, and P90 rates.

In the EnLU procedure, the majority of the computation is associated with the simulation of fine-scale models, as required for the global upscaling procedure. Although we would like to perform as few fine-scale simulations as possible, coarse-model accuracy will degrade if too few fine-scale runs are performed. We now investigate the impact of using only five globally upscaled models (each of which requires global compositional simulation) instead of ten models, as were used in previous results. The P10, P50, and P90 curves for field oil and gas rates using EnLU with five globally upscaled models are shown in Fig. 15. These results are not as accurate as EnLU results based on ten upscaled models (Figs. 10c and 11c), though they still provide significant improvement over standard coarse models (Figs. 10a and 11a). In future work, it will be useful to develop procedures to estimate the required number of globally upscaled models to use in EnLU.

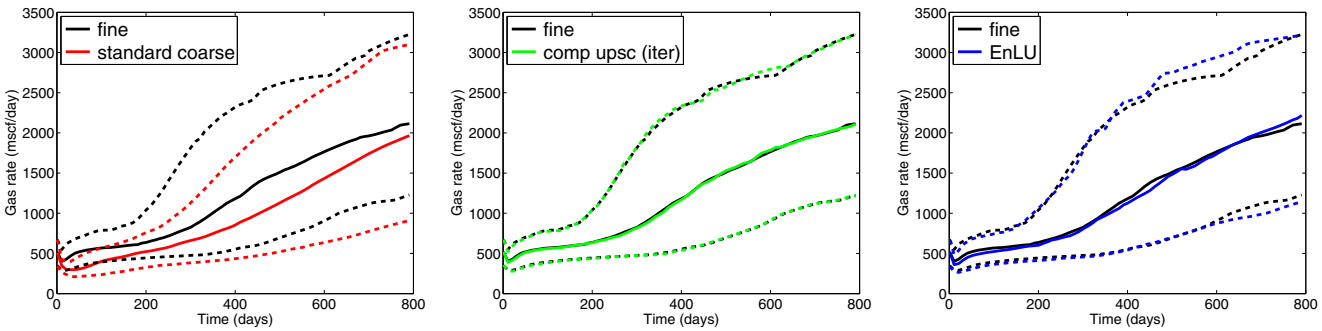

(a) Standard coarse (b) Full upscaled (c) EnLU (10% sim.)

Fig. 18 P10, P50, and P90 curves for gas field production rate (channelized permeability field)

All simulation runs in this work were performed on a PC with Intel Core2 Duo CPU (2.66 GHz). A single fine-scale simulation for this case entails over 3 h of computation time. The computation of T^*, plus the calculation of k^*_{rj} and the initial estimate of α_{ij} from the fine-scale results, requires a total of about 10–15 s. The iteration procedure applied to compute improved α_{ij} requires another 1–2 min. The coarse-model simulation is achieved in about 30 s. Thus, nearly all of the computation corresponds to the fine-scale compositional simulations. The speedup achieved through use of EnLU, relative to performing fine-scale simulation on all models, is essentially just the ratio of the number of fine-scale simulations required by the two approaches. Thus, for an ensemble of 100 realizations, when using EnLU with ten globally upscaled models, we achieve a speedup factor of about 10, and when five globally upscaled models are used, we achieve a speedup factor of about 20.

5.2 Channelized permeability fields

We now apply the EnLU procedure for more complex models characterized by channelized permeability fields. All realizations were generated using Stanford Geostatistical Modeling Software, SGeMS [39]. The permeability distributions ($\log k$) for three realizations are shown in Fig. 16. A five-spot well pattern with one injector and four producers is again used. The models are conditioned such that the injection well always penetrates mud (to avoid very fast breakthrough). The fine-scale model contains 55×55 grid blocks, with each block of dimensions 50 ft $\times$ 50 ft $\times$ 10 ft. The coarse-scale model, generated by uniformly coarsening the fine model, contains 11×11 blocks. We take $k_x = k_y$ for each fine-scale cell. Porosity is prescribed to be constant at a value of 0.25.

For this case, we inject pure CO_2 into a four-component system initially containing C_1 (20 %), CO_2 (1 %), C_4 (29 %), and C_{10} (50 %). The reservoir is at a constant temperature of 350 K and an initial pressure of 1050 psi. The injection well operates at a pressure of 1500 psi, and the production wells at a pressure of 500 psi. The simulation period is 800 days.

Results for P10, P50, and P90 field oil and gas production rates are shown in Figs. 17 and 18. Our general observations regarding the relative accuracy of the three procedures are consistent with those in the previous case. We again see that EnLU provides results that are nearly as accurate as those from full flow-based upscaling, but with only 10 % of the upscaling effort. This again highlights the potential applicability of EnLU for uncertainty quantification in challenging compositional problems. The speedup achieved using EnLU for this case is about a factor of 10, with the timings dominated by the fine-scale compositional simulations, as in the previous example. EnLU results for additional systems are presented in [30].

6 Concluding remarks

In this paper, we presented an ensemble level upscaling procedure for compositional flow simulation. The underlying iterative-global upscaling technique entails the computation of upscaled transmissibilities, relative permeabilities, and α-factors for each coarse-scale interface. Coarse-scale iteration on α-factors provides improved accuracy at low cost relative to the global fine-scale simulation required for the upscaling. We defined appropriate attributes for use in the EnLU calibration step. The spatial correlation structure of upscaled two-phase flow functions was quantified via variogram modeling, and this structure was then used within a sequential Gaussian co-simulation framework. This enables the coarse-scale functions assigned in EnLU to approximately honor the spatial correlation structure observed in realizations for which flow-based upscaling was applied.

We illustrated the high degree of accuracy of the iterative global upscaling method for a single realization of a two-dimensional Gaussian permeability field. EnLU was then applied to compositional problems involving gas injection into four-component systems. Both Gaussian and channelized permeability fields were considered. It was shown that the use of standard upscaling (T^* and WI^* only) led to substantial errors for the cases considered. Global compositional upscaling, by contrast, yielded coarse results of very high accuracy. The use of EnLU was shown to provide models that closely matched the flow statistics (P10, P50, P90) of the fine-scale production rates. In fact, accuracy close to that from global compositional upscaling was achieved. EnLU also improved the realization-by-realization agreement significantly compared to using standard coarse models, though its accuracy was not as high as that from full flow-based upscaling.

There are a number of issues that should be considered in future work. Rather than apply global compositional upscaling, more efficient local-global upscaling [30], or a combination of local-global and global approaches, could be incorporated into the EnLU framework. This could improve the overall computational efficiency significantly. The use of different or additional attributes (e.g., time of flight) in EnLU should also be investigated. This, along with specialized techniques for determining the required number of realizations and selecting particular realizations for global upscaling, could lead to improved performance and/or better efficiency. Finally, our procedures should be extended to treat models that are more complex in terms of both

grid geometry and fluid systems. At that point, the methods presented in this paper should be applicable for practical cases.

Acknowledgements We thank the Stanford University Reservoir Simulation Research Industrial Affiliates Program (SUPRI-B) for financial support. We are grateful to Denis Voskov and Rustem Zaydullin for useful discussions on constructing the compositional models, to Huanquan Pan for assistance with GPRS, and to Hai Vo for help with SGeMS.

References

1. White, C.D., Horne, R.N.: Computing absolute transmissibility in the presence of fine-scale heterogeneity, 1987. Paper SPE 16011 presented at the SPE Reservoir Simulation Symposium, San Antonio
2. Zhang, P., Pickup, G.E., Christie, M.A.: A new practical method for upscaling in highly heterogeneous reservoir models. SPE J. **13**, 68–76 (2008)
3. Chen, Y., Mallison, B.T., Durlofsky, L.J.: Nonlinear two-point flux approximation for modeling full-tensor effects in subsurface flow simulations. Comput. Geosci. **12**, 317–335 (2008)
4. Chen, T., Gerritsen, M.G., Lambers, J.V., Durlofsky, L.J.: Global variable compact multipoint methods for accurate upscaling with full-tensor effects. Comput. Geosci. **14**, 65–81 (2010)
5. Chen, Y., Durlofsky, L.J.: Efficient incorporation of global effects in upscaled models of two-phase flow and transport in heterogeneous formations. Multiscale Modeling & Simulation **5**, 445–475 (2006)
6. Chen, Y., Li, Y.: Local-global two-phase upscaling of flow and transport in heterogeneous formations. Multiscale Modeling & Simulation **8**, 125–153 (2009)
7. Durlofsky, L.J., Chen, Y.: Uncertainty quantification for subsurface flow problems using coarse-scale models. In: Graham, I.G., Hou, T.Y., Lakkis, O., Scheichl, R. (eds.) Numerical Analysis of Multiscale Problems, Lecture Notes in Computational Science and Engineering, vol. 83, pp. 163–202. Springer (2012)
8. Barker, J.W., Thibeau, S.: A critical review of the use of pseudorelative permeabilities for upscaling. SPE Reserv. Eng. **12**, 138–143 (1997)
9. Barker, J.W., Dupouy, P.: An analysis of dynamic pseudo-relative permeability methods for oil-water flows. Pet. Geosci. **5**, 385–394 (1999)
10. Darman, N.H., Pickup, G.E., Sorbie, K.S.: A comparison of two-phase dynamic upscaling methods based on fluid potentials. Comput. Geosci. **6**, 5–27 (2002)
11. Suzuki, K., Hewett, T.A.: Sequential upscaling method. Transp. Porous Media **46**, 179–212 (2002)
12. Ding, Y.: Scaling-up in the vicinity of wells in heterogeneous field, 1995. Paper SPE 29137 presented at the SPE Reservoir Simulation Symposium, San Antonio
13. Durlofsky, L.J., Milliken, W.J., Bernath, A.: Scaleup in the near-well region. SPE J. **5**, 110–117 (2000)
14. Muggeridge, A.H., Cuypers, M., Bacquet, C., Barker, J.W.: Scale-up of well performance for reservoir flow simulation. Pet. Geosci. **8**, 133–139 (2002)
15. Hui, M., Durlofsky, L.J.: Accurate coarse modeling of well-driven, high-mobility-ratio displacements in heterogeneous reservoirs. J. Pet. Sci. Eng. **49**, 37–56 (2005)
16. Nakashima, T., Durlofsky, L.J.: Accurate representation of near-well effects in coarse-scale models of primary oil production. Transp. Porous Media **83**, 741–770 (2010)
17. Nakashima, T., Li, H., Durlofsky, L.J.: Near-well upscaling for three phase flows. Comput. Geosci. **16**, 55–73 (2012)
18. Li, H., Chen, Y., Rojas, D., Kumar, M.: Development and application of near-well multiphase upscaling for forecasting of heavy oil primary production. J. Pet. Sci. Eng. **113**, 81–96 (2014)
19. Camy, J.P., Emanuel, A.S.: Effect of grid size in the compositional simulation of CO_2 injection, 1977. Paper SPE 6894 presented at the SPE Annual Fall Technical Conference and Exhibition, Denver
20. Fayers, F.J., Barker, J.W., Newley, T.M.J.: Effects of heterogeneities on phase behaviour in enhanced oil recovery. In: Proceedings of the 1^{st} European Conference on the Mathematics of Oil Recovery, Cambridge (1989)
21. Barker, J.W., Fayers, F.J.: Transport coefficients for compositional simulation with coarse grids in heterogeneous media. SPE Adv. Technol. Ser. **2**, 103–112 (1994)
22. Christie, M.A., Clifford, P.J.: Fast procedure for upscaling compositional simulation. SPE J. **3**, 271–278 (1998)
23. Ballin, P.R., Clifford, P.J., Christie, M.A.: Cupiagua: modeling of a complex fractured reservoir using compositional upscaling. SPE Reserv. Eval. Eng. **5**, 488–498 (2002)
24. Ogunlana, D.O., Mohanty, K.K.: Compositional upscaling in fractured reservoirs during gas recycling. J. Pet. Sci. Eng. **46**, 1–21 (2005)
25. Salehi, A., Voskov, D.V., Tchelepi, H.A.: Thermodynamically consistent transport coefficients for upscaling of compositional processes, 2013. Paper SPE 163576 presented at the SPE Reservoir Simulation Symposium, The Woodlands
26. Iranshahr, A., Chen, Y., Voskov, D.V.: A coarse-scale compositional model. Comput. Geosci. **18**, 797–815 (2014)
27. Chen, Y., Durlofsky, L.J.: Ensemble-level upscaling for efficient estimation of fine-scale production statistics. SPE J. **13**, 400–411 (2008)
28. Chen, Y., Park, K., Durlofsky, L.J.: Statistical assignment of upscaled flow functions for an ensemble of geological models. Comput. Geosci. **15**, 35–51 (2011)
29. Suzuki, S.: Pattern-based approach to multiphase flow upscaling using distance-based clustering, 2011. Paper SPE 146639 presented at the SPE Annual Technical Conference and Exhibition, Denver
30. Li, H.: Compositional Upscaling for Individual Models and Ensembles of Realizations. PhD thesis, Stanford University (2014)
31. Li, H., Durlofsky, L.J.: Upscaling for compositional reservoir simulation, 2015. Paper SPE 173212 presented at the SPE Reservoir Simulation Symposium, Houston
32. Cao, H.: Development of Techniques for General Purpose Simulators. PhD thesis, Stanford University (2002)
33. Jiang, Y.: Techniques for Modeling Complex Reservoirs and Advanced Wells. PhD thesis, Stanford University (2007)
34. Deutsch, C.V., Journel, A.G. GSLIB: Geostatistical Software Library and User's Guide, 2nd edn. Oxford University Press, New York (1998)
35. Orr, F.M.: Theory of Gas Injection Processes. Tie-Line Publications (2007)
36. Dupouy, P., Barker, J.W., Valois, J.P.: Grouping pseudo relative permeability curves. In Situ **22**, 1–33 (1998)
37. Durlofsky, L.J.: Coarse scale models of two phase flow in heterogeneous reservoirs: volume averaged equations and their relationship to existing upscaling techniques. Comput. Geosci. **2**, 73–92 (1998)
38. Gringarten, E., Deutsch, C.V.: Teacher's aide variogram interpretation and modeling. Math. Geol. **33**, 507–534 (2001)
39. Remy, N., Boucher, A., Wu, J.: Applied Geostatistics with SGeMS: a User's Guide. Cambridge University Press, New York (2009)